# Impact of media coating on simultaneous manganese removal and remineralization of soft water via calcite contactor

Hamed Pourahmad[1], Maryam Haddad[1], Dominique Claveau-Mallet[2] and Benoit Barbeau[1*].

1: Department of Civil, Geological & Mining Engineering, Ecole Polytechnique de Montréal, 2900 boulevard Édouard-Montpetit, Montréal, Québec, Canada H3T 1J4,

2: Department of Chemical Engineering, McGill University, 3610 University Street, Montréal, Québec H3A 0C5, Canada,

* corresponding author: Benoit Barbeau (benoit.barbeau@polymtl.ca)

## Abstract

The aim of this study was to investigate the negative impact of a newly-formed manganese (Mn)-layer on calcite dissolution in the long-term operation of a calcite contactor. Simultaneous removal of Mn and remineralization of soft water in an up-flow calcite contactor was conducted and led to a progressive loading of Mn into the calcite matrix. The calcite contactor demonstrated high Mn removal; however, the hardness release decreased from 32 to 20 mg $CaCO_3$ $L^{-1}$ after 600 h of operation on a high Mn concentration (5 mg $L^{-1}$) feed. For an elevated Mn concentration (i.e. 5 mg Mn $L^{-1}$) in the feed water, the coated layer was mainly composed of Mn which inhibits the mass transfer from the calcite core to the liquid phase. The superficial layer was identified as 5.2% Mn oxides (MnOx) by X-ray photoelectron spectroscopy (XPS). Therefore, it is postulated that Mn removal starts with an ion exchange sorption reaction between soluble $Mn^{2+}$ from aqueous phase and $Ca^{2+}$ from the $CaCO_3$ matrix which is followed by a slow recrystallization of $MnCO_3$ into

$MnO_2$. On the other hand, when the Mn content in the feed water was lower (i.e. 0.5 mg Mn $L^{-1}$), a considerably lower amount of MnOx was detected on the coated media. For all the examined conditions, the formation of this coating improved Mn removal due to the autocatalytic nature of the adsorption/oxidation of dissolved manganese by MnOx. A mechanistic model based on calcite dissolution and the progressive formation of a $MnO_2$ layer was implemented in PHREEQC software to predict the reduction in hardness release expected in long-term operation. The model was calibrated with experimental data and resulted in realistic breakthrough curves. In order to accurately predict the pH of the effluent stream, a slow-rate recrystallization of $MnCO_3$ into $MnO_2$ was implemented (compared to the fast precipitation of $MnO_2$ or the absence of $MnO_2$ formation).

## Keywords

Calcite Contactor, Manganese Removal, Soft water Remineralization, Groundwater supplies, sorption, PHREEQC

## 1. Introduction

Corrosion control is an important water treatment objective. Addition of caustic soda, soda ash, lime (with or without carbon dioxide) and various corrosion inhibitors are the main corrosion control techniques used in municipal water treatment sector (Withers, 2005). For domestic purposes and small water systems, filtration through a bed made of calcite (i.e. calcium carbonate often referred to as a calcite or limestone contactor) is a common passive strategy to raise the pH and alkalinity of treated waters. Remineralization of the finished water from desalination plants is another common application of this process. Calcite dissolution, as described by Eq. 1, provides calcium hardness and bicarbonate alkalinity.

$$CaCO_3 + CO_2 + H_2O \rightarrow Ca^{2+} + 2\ HCO_3^- \quad \text{(Eq. 1)}$$

Several researches have shown that calcite filtration is a reliable remineralization method as no continuous chemical addition is required and calcite is inexpensive, readily available, safe to handle and easy to store (Shemer et al., 2013, Van Der Laan. H., 2016). Another interesting advantage of calcite lies in its ability to sorb divalent metallic cations ($Me^{2+}$) on its surface (Aziz and Smith, 1996, Franklin and Morse, 1983). A number of researchers recommended using calcite media for manganese removal from acid mine drainage (Aziz and Smith, 1992, Aziz and Smith, 1996, Thornton, 1995, Zachara et al., 1991). In drinking water applications, manganese removal is also a common treatment objective. The occurrence of Mn in drinking water causes aesthetic and operational issues (Tobiason et al., 2016). Manganese is under review in Canada and the USA for a possible health-based regulation given the increased evidence of manganese neurotoxicity, especially for children (Bouchard et al., 2011, Dion et al., 2018). Thus, effective removal of Mn from drinking water is crucial.

Mn removal from drinking water sources can be carried out by different methods (Tobiason et al., 2016). A common municipal water treatment technique for Mn removal relies on its oxidation by a strong chemical followed by precipitation and particle removal (Kothari, 1988). As on-line chemical injection is challenging in small-scale applications, point-of-entry (POE) catalytic filtration with intermittent regeneration or POE cationic ion exchange (IX) coupled with point-of-use reverse osmosis are two widely implemented options to remove Mn in domestic applications (Carrière et al., 2011). Nonetheless, the risk of Mn leaching from improperly operated catalytic filters, the high salt consumption for IX regeneration and the considerable amount of brine waste production, which pollutes the environment, are common drawbacks of these methods (Barbeau et al., 2011, Carrière et al., 2011). As an alternative, we recently proposed the use of chlorine resistant

and back-washable hollow fiber nanofiltration (HFNF) membranes for the removal of Mn from domestic groundwater supplies (Haddad et al., 2018). We concluded that even though HFNF application can be an appealing solution for the removal of Mn and Fe, non-selective rejection properties of the HFNF membranes would result in a corrosive treated water. Therefore, the HFNF process should be coupled with a polishing step, such as a calcite contactor, to adjust the hardness level of its soft permeate. This final post-treatment can also further reduce the dissolved Mn traces which were not completely rejected by the HFNF membranes (Haddad et al., 2018).

Calcite ($CaCO_3$)-Mn interaction and particularly the fate of various phases in the complex system of $CaCO_3$-$MnCO_3$-$H_2O$ has been extensively documented in the literature (McBride, 1979, Pingitore et al., 1988, Franklin and Morse, 1983, Kothari, 1988, Silva et al., 2012b, Thornton, 1995, Zachara et al., 1991). In 2010, Silva et al. studied the interaction of $Mn^{2+}$ and calcite and claimed that the nucleation of the discrete phase of rhodochrosite (i.e., $MnCO_3$) takes place at the surface of the calcite media (Silva et al., 2010). By contrast, a number of researchers indicated that a dilute solid solution of $Mn^{2+}$-$CaCO_3$ is formed at the surface due to the displacement of $Mn^{2+}$ in the calcite matrix (Pingitore et al., 1988, McBride, 1979, Comans and Middelburg, 1987). Furthermore, since no adsorption maximum is determined in the abovementioned studies, it can be deduced that both precipitation and adsorption were involved during the interaction between Mn and calcite (McBride, 1979). The most commonly accepted kinetic rate law for Mn and calcite interaction includes an initial rapid uptake of the trace metal (i.e. $Mn^{2+}$) followed by a relatively slow formation of a solid solution expressed as $Mn_{(x)}Ca_{(1-x)}CO_{3;}$ where the composition (x) changes between the original solid and precipitate of the sorbate while it is gradually formed (Farley et al., 1985, McBride, 1979, Zachara et al., 1991). The initial rapid step is generally linked to an adsorption reaction while the following slow uptake is mainly attributed to the formation of

solid solution and removal by surface precipitation. A number of researchers claimed that at a low aqueous concentration, metals only incorporate into the surface of calcite by adsorption with no solid solution formation (Zachara et al., 1991, Franklin and Morse, 1983, Comans and Middelburg, 1987, McBride, 1979). In 1991, Zachara and coworkers reported that metals with ionic radii smaller than Ca were more prone to sorb on calcite (Zachara et al., 1991) which favors the theory of calcium displacement. Finally, it should be noted that $Mn^{2+}$, once integrated into the solid matrix of calcite, exhibits a very slow desorption rate (induced by lowering pH from 8.7 to 7.6) which favors the application of calcite for Mn sorption in the field of water treatment (Zachara et al., 1991).

The three most common calcite dissolution models are Plummer, Parkhurst, Wigley (PWP) (1978) Yamauchi (1987) and Letterman (1987) (Plummer et al., 1979, Plummer et al., 1978, Yamauchi et al., 1987, Letterman et al., 1987). In the PWP and Yamauchi models, it is assumed that the flow is turbulent and the process is very fast; thereby, the calcite dissolution is controlled only by surface reactions, i.e., diffusional mass transport is neglected (Ghanbari, 2018, Plummer et al., 1979, Yamauchi et al., 1987). On the other hand, in the Letterman model, mass transfer is the key controlling mechanism used to predict calcite dissolution (Letterman et al., 1987). However, none of these models account for the potential negative impact on calcite dissolution arising from the precipitation of manganese on its surface. Despite the fact that there are several comprehensive studies pertaining to both the implementation of calcite contactors as a reliable and straightforward remineralization and corrosion control technique and Mn adsorption on the surface of calcite, to the best of our knowledge, the significance and fate of sorbed Mn on the overall performance of a calcite contactor in long-term operation has not received enough attention. In this regard, the primary goal of this research effort is to determine the effect of Mn-coating on the calcite

dissolution rate and to model the long-term behavior of a calcite contactor operated for drinking water remineralization. The outcome of this study enables us to gain a clear insight of the fate and significance of sorbed Mn at the calcite surface and helps in the design of a simple and effective polishing step for the soft permeate from the HFNF processes.

## 2. Materials and methods

### 2.1. Calcite media and synthetic feed water

Synthetic feed water (SFW) was prepared by dissolving analytical grade (>99% pure) $MnSO_4$ (Fisher Scientific, NJ, USA) in aerobic ultra-pure (i.e., Milli-Q™) water resulting in an acidic influent water (pH of 5.7-6.0). Commercially available calcite (2.68 g/cm$^3$) media was purchased from Imerys Marble Inc. (Sahuarita, AZ, USA) and then dry-sieved to calculate the median diameter ($D_{50}$). The main characteristics of calcite media are summarized in Table 1.

Table 1: Calcite media characteristics

| **Filter media** | **$D_{50}$ (1) (mm)** | **Purity (2) (%)** | **Specific gravity (3) (g/cm$^3$)** | **Bulk density (3) (kg/m$^3$)** | **Porosity (3) ($\varepsilon$)** | **Surface area (4) (m$^2$/g)** | **Other impurities (3)** |
|---|---|---|---|---|---|---|---|
| Calcite ($CaCO_3$) | 0.4 | 99.70 | 2.68 | 1 500 | 0.42 | 0.371 | 0.3 % Mg |

(1) Measured in the laboratory using sieving
(2) Determined by Inductively Coupled Plasma-Optical Emission Spectrometry (ICP-OES, model iCAP 6000, Thermo Instruments Inc) after nitric acid acidification
(3) Provided by the supplier (Imerys Marble Inc, Sahuarita, AZ, USA)
(4) Data provided via BET measurement (the BET procedure is described in (Gambou-Bosca and Bélanger, 2016))

### 2.2. Experimental design

Two consecutive experimental phases and a single modeling phase were adopted. In the first phase, we determined the overall performance of a calcite contactor for the removal of Mn and the

remineralization of SFW using two initial concentrations of Mn (i.e. 0.5 and 5 mg Mn $L^{-1}$). Based on the results obtained from this phase, the objective of the second phase was to investigate the effect of Mn solid-phase concentration on the calcite dissolution rate using continuous desorption-dissolution experiments in smaller columns. To this end, we transferred the media from the loaded column used for the first phase to 4 mini-columns and operated them for five days in a continuous mode while feeding them with ultra-pure water. As for the final phase, the long-term effectiveness of a calcite contactor was modeled based on calcite dissolution, Mn precipitation and filter clogging. The model was implemented in PHREEQC.

### 2.3. Continuous sorption-dissolution experiments

In Phase 1, sorption-dissolution experiments were conducted on calcite media in order to assess the effectiveness of a calcite contactor for both remineralization and partial Mn removal. The assays were carried out at room temperature (i.e. 23 ± 2 °C) in two parallel cylindrical acrylic columns (1.3 m height and 31.75 mm internal diameter) filled to a height of 80 cm with fresh calcite media and continuously fed up-flow with SFW containing 0.5 mg Mn $L^{-1}$ (column A) or 5 mg Mn $L^{-1}$ (column B), respectively. The flow rate was set at 30 mL $min^{-1}$ which translates into an up-flow velocity of 2.27 m $h^{-1}$ and empty bed contact times (EBCT) of 10 min in the second valve (at height of 40 cm) and 20 min in the effluent. It should be noted that these concentrations represent either high or very high Mn conditions in groundwater supplies (Canada, 2016). A schematic illustration of the sorption-dissolution set-up is shown in Fig. 1. Throughout the sorption-dissolution assays, samples were collected from four sampling points located at different heights and therefore representing increasing EBCTs. Samples were analyzed to determine Mn concentration, pH and hardness, immediately after their collection. Hardness was measured by

titration (Standard methods, Hardness (2340)/EDTA Titrimetric Method) while acidified manganese samples were analyzed by ICP-AES (Thermo-Fisher, ICAP 6000). Details of the ICP sample preparation and the applied measurement procedure can be found elsewhere (Haddad et al., 2018).

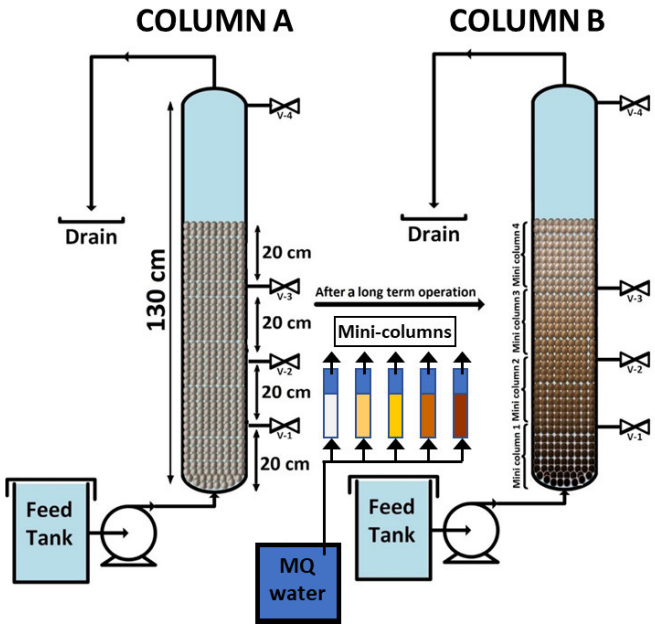


Figure 1: Schematic illustration of the continuous upflow sorption-dissolution set-up. Feed water: Column A= 0.5 mg Mn/L & Column B = 5.0 mg Mn/L. After 800 h of operation, media from column B was recovered at four columns depths (see right column) and transferred into mini-columns which were fed with MilliQ water to assess the impact of Mn solid-phase concentration on Mn and calcium release.

### 2.4. Characterisation of calcite Mn-loaded media

After long-term operation (approximately 800 h) of the sorption-dissolution columns, samples of Mn-loaded calcite media were collected from different depths of column B for further analysis. Scanning Electron Microscope (SEM), Energy Dispersive X-ray Analysis (EDX) and X-ray Photoelectron Spectroscopy (XPS) were used to characterize the media before and after loading and to determine the nature of the deposits found over the surface (Detailed description of the

analytical methods are provided in the appendix). To determine the Mn solid-phase concentration on the calcite, pre-weighed samples (160 mg) of dried, loaded media (with different Mn content) were digested in 15 mL of 10% (wt.) $HNO_3$. Following a complete dissolution, Mn concentrations were measured by means of an ICP-AES.

### 2.5. Continuous desorption experiment and impact of Mn coating on calcite dissolution

In order to investigate the Mn desorption rate, column B (Fig. 1) was fed with Milli-Q water for 120 h and samples were collected from two sampling points located at different heights and therefore representing increasing EBCTs (i.e. 10 and 20 min). In addition, the impact of Mn solid-phase concentration on calcite dissolution and Mn sorption was tested by transferring to five mini-columns (20 cm media height and 1.5 cm internal diameter) four subsamples of column B media selected with increasing Mn solid-phase concentrations ranging from 0 to 15 mg Mn $g^{-1}$ of media (Table 3). The first column contained fresh calcite media and was considered as the control case. The mini-columns were fed at 1.2 m $h^{-1}$ with Milli-Q water for 72 h. Samples were frequently taken from the influent/effluents and characterized for Mn content, hardness level and pH according to the methods described above.

Table 2: Mn solid-phase concentrations present on the media installed in the different mini-columns

| # Columns | Column 1* | Column 2 | Column 3 | Column 4 | Column 5 |
|---|---|---|---|---|---|
| Mn content of the media (mg Mn/g media) | 0.004 | 1.06 | 2.13 | 4.02 | 15.0 |
| Visual aspect of the loaded media |  |  |  |  |  |

* The control column is with fresh calcite media

### 2.6. Batch sorption experiments on Mn-loaded media

Experiments were carried out at T = 23ºC to study the effect of Mn solid-phase concentration on calcite dissolution and to investigate the ability of the highly Mn-loaded calcite (collected from the bottom of the large column, i.e. column B in Fig. 1) in further removal of $Mn^{2+}$. The sorption studies were performed by adding 10 g $L^{-1}$ of Mn-loaded media to 200 mL flasks with various $Mn^{+2}$ concentrations (0.0, 0.1, 1.0 and 10 mg Mn $L^{-1}$). Throughout the sorption assays, the flasks were shaken (using Max Q2508 Thermo-Fisher shaker) at 150 rpm. At predetermined contact times (i.e. 15 m, 1 h, 12h, 24 h, 48 h and 7d), a flask from each Mn concentration was removed, settled for 1-min and the supernatant was filtered using a 0.45 μm membrane filter (Supor ®PES Membrane Disc Filters, Pall, US) prior to taking Mn, hardness and pH measurements.

### 2.8. Model description and numerical simulations

The applied model in this study consisted of the equations for calcite dissolution, $MnCO_3$ formation (by ionic exchange between $Ca^{2+}$ and $Mn^{2+}$) as well as the slow recrystallization of $MnCO_3$ into $MnO_2$ as indicated in Table 3. In this regard, a simple calcite dissolution rate was defined based on the calcite saturation index. In Claveau-Mallet et al. (2017), the successful application of the selected rate is reported for phosphorus precipitation in granular reactors. The calcite equilibrium constant was set at $pK_{spCAL} = 8.48$ according to a standard geochemical database for crystalline calcite (Parkhurst and Appelo, 1999). The formation of $MnO_2$ was assumed according to mineralogical observations performed in this study (presented in the results section). The $MnCO_3$ precipitation rate was set as a first order reaction without $MnCO_3$ saturation, assuming that autocatalytic sorption took place onto previously formed seeds. The $MnCO_3$ precipitation kinetic constant was increasing gradually to account for the increase of seeds. A saturation term of $1.8 \times 10^{-7}$ M (10 µg Mn $L^{-1}$) was included in the rate to represent the lowest residual concentration observed in the effluent of the calcite contactor.

Calcite dissolution was presumed to be progressively limited by the formation of a thin $MnO_2$ film over the calcite grains. The diffusion of $Ca^{2+}$ and $CO_3^{2-}$ ions through the film was modelled based on Fick's law. At each iteration step, both dissolution and diffusion rates were calculated, and only the smallest rate was applied (which resulted in dissolution control at first and diffusion control afterward).

Table 3: Applied equations for modeling calcite dissolution and manganese removal

| Processes | Stoichiometry | | | | | Rate law |
|---|---|---|---|---|---|---|
| | $Ca^{2+}$ | $CO_3{}^{2-}$ | $Mn^{2+}$ | $H^+$ | $e^-$ | |
| Calcite dissolution | -1 | -1 | | | | $r_{CAL} = k_{CAL} log\left(\frac{\{Ca^{2+}\}\{CO_3{}^{2-}\}}{K_{spCAL}}\right)$ |
| Calcite diffusion through $MnO_2$ thin film | -1 | -1 | | | | $r_{diff} = \frac{0.001 D_{barr}\left(K_{spCAL} - \{Ca^{2+}\}\{CO_3{}^{2-}\}\right)}{d_{barr}}\left(\frac{S0.001(1-n)}{n}\right)$ |
| $MnCO_3$ formation by ionic exchange from calcite matrix | +1 | | -1 | | | $r_{MnCO3} = k_{MnCO3}([Mn^{2+}] - 1.8 \times 10^{-7})$ $k_{MnCO3} = 10^{(A * X_{Mn} - B)}$ Note: $1.8 \times 10^{-7}$ is a saturation term describing the min concentration of $Mn^{+2}$ (based on experimental measurements) |
| Recrystallization of $MnCO_3$ into $MnO_2$ | | +1 | | +4 | +2 | $r_{MnO2} = k_{MnO2}([MnCO_3] - [MnO_2])$ |

$X_{Mn}$: total Mn precipitated in the calcite contactor (mol $L^{-1}$ void volume); $A$ and $B$: constants for seeding; $D_{barr}$: diffusion coefficient in the thin film ($m^2/s$); $d_{barr}$: thickness of the thin film (m) assuming a dry density of $MnO_2$ crystals of $2\times10^6$ $g/m^3$ in the thin film; $S$: calcite sand surface area ($m^2/m^3$); $n$: total porosity in the calcite contactor (adimensional); $Ca_{eq}$: calcium concentration at equilibrium with calcite at the grain surface.

The model was implemented in the PHREEQC software using a MATLAB interface via IPHREEQC modules (Charlton and Parkhurst, 2011). The equations from Table 4 were written in the RATES and KINETICS datablock with $1.0 \times 10^{-6}$ solving tolerance. The calcite contactor was simulated using the TRANSPORT datablock. Hydraulic properties were defined following the PHREEQC dual porosity feature: with a mobile porosity of 34%, an immobile porosity of 1.2%, a dispersivity of 5 cm and an exchange factor of $5.0 \times 10^{-6}$ $s^{-1}$. These hydraulic properties were selected based on typical hydraulic behavior of sand columns (Domenico and Schwartz, 1998). The simulated column had 8 cells. The influent was simulated in the REACTION datablock in which $CaCl_2$, $MnSO_4$ and $NaHCO_3$ were added to reproduce the experimental conditions. Prior to the column simulation, the influent was equilibrated with calcite and with a 300 ppm $CO_2$ atmosphere. The model kinetic constants $k_{CAL}$, $k_{MnCO3}$ and $k_{MnO2}$ as well as diffusion coefficient $D_{barr}$ were calibrated using the data from the continuous sorption-dissolution experiment. The

calibrated model was used for scenario simulations with different influent manganese concentrations and different precipitation hypotheses.

# 3. Results and discussion

## 3.1. Media characterization

The fresh calcite and loaded calcite produced in the long-term operation of the contactor fed with 5 mg Mn $L^{-1}$ were characterized by SEM, EDX and XPS. Fig. 2 depicts the SEM images of the calcite surface before and after Mn sorption at 1000X as well as EDX results obtained at 250X magnification. SEM images show the structure of the coating at the calcite surface. By comparing the SEM images of the fresh and Mn loaded media, one can note that the loaded media exhibited a smoother surface. The EDX results demonstrated no Mn peak in fresh media (0%); whereas a gradual increase in the Mn content (≤ 15%) of the loaded media was observed. Thus, it can be presumed that the Mn was progressively coated on the calcite surface, forming a layer of Mn which can inhibit the mass transfer from the calcite core to the liquid phase.

The nature of the newly formed residue was investigated by XPS analysis. Even though the Mn2p3 peak for $MnCO_3$ is expected at a binding energy (BE) around 640.4 eV (Table 4 an Appendix) (Baer et al., 1991), the Mn2p3 peak was observed at a BE of 641.7 eV which corresponds to the $Mn^{3+}$ and $Mn^{4+}$ oxides and hydroxides. It should be noted that a number of researchers reported the incorporation of Mn into the calcite matrix and the formation of $MnCO_3$ (Silva et al., 2010, Silva et al., 2012b, Silva et al., 2012a, Pingitore et al., 1988); however, based on the XPS results, the newly formed residue was not solely $MnCO_3$, as the presence of Mn oxides and hydroxides were detected at the calcite surface. The detection of MnOx formation on the surface was supported by the pH measurements in the effluent which were lower than what would have been expected in

the case of sole formation of $MnCO_3$. The formation of MnOx is expected to slightly acidify the effluent. Therefore, it was postulated that Mn sorption starts with an ion exchange reaction between soluble $Mn^{2+}$ from aqueous phase and $Ca^{2+}$ from the $CaCO_3$ matrix which is followed by slow recrystallization of $MnCO_3$ into $MnO_2$.

| Media specifications | SEM image (1000X) | EDX Spectrum (250X) |
|---|---|---|
| Mini-column #1 (Control case) (0 mg Mn $g^{-1}$ calcite) | 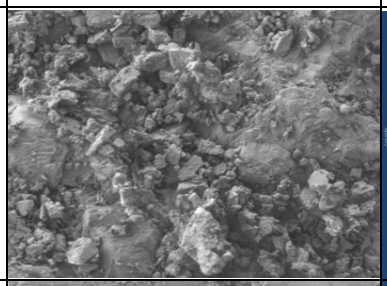 | 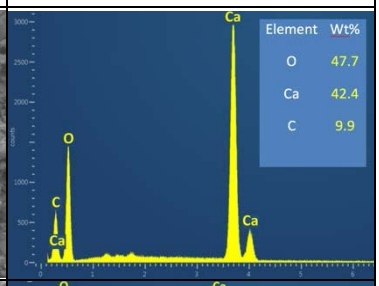  |
| Mini-column #2 (1.06 mg Mn $g^{-1}$ calcite) | 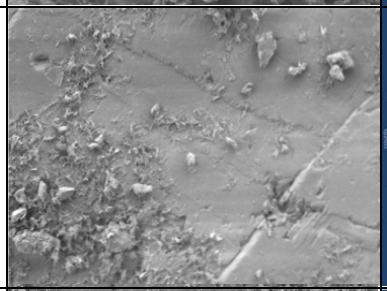 | 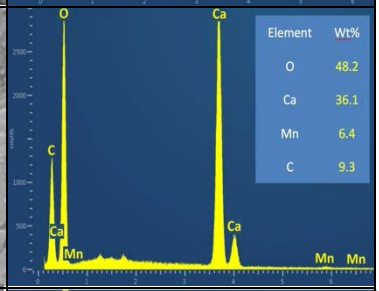  |
| Mini-column #3 (2.13 mg Mn $g^{-1}$ calcite) | 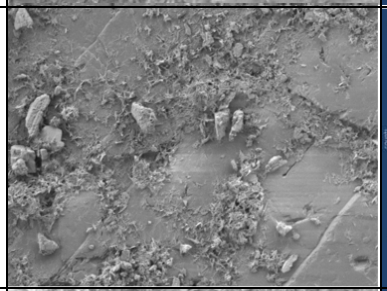 | 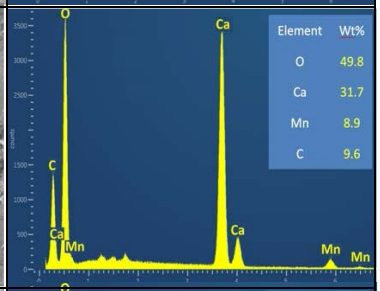  |
| Mini-column #4 (4.02 mg Mn $g^{-1}$ calcite) | 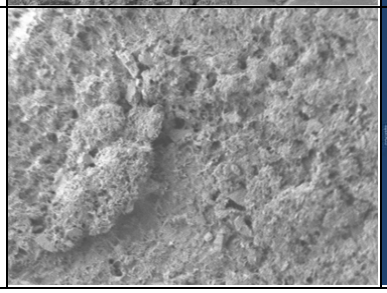 | 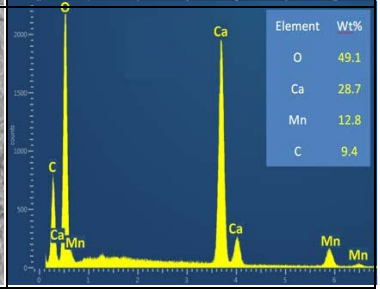  |

| | | |
|---|---|---|
| Mini-column #5 (15.0 mg Mn $g^{-1}$ calcite) | 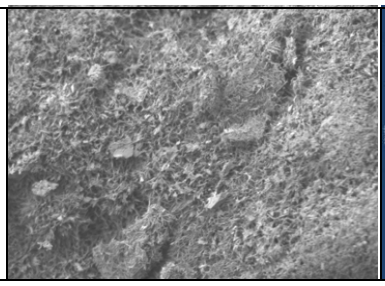 | 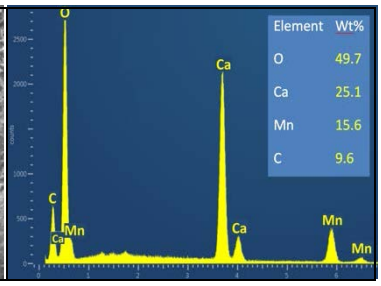  |

Figure 2: SEM images and EDX analyses of calcite media obtained from different Mn solid-phase concentrations on the calcite media.

Table 4: High resolution XPS spectra for Mn loaded calcite

| Name | BE (eV) | Identification | Relative atomic % | |
|---|---|---|---|---|
| | | | **Fresh calcite** ≈ 0 mg/g | **Mn-loaded calcite** 15 mg/g sample |
| **C1s** | 285.0 | C-C | 15.7 | 11.5 |
| | 288.7 | O-C=O | 1.2 | 2.4 |
| | 290.1 | R-$CO_3$ | 12.9 | 10.7 |
| **Ca2p3** | 347.3 | $CaCO_3$ | 12.7 | 12.0 |
| **O1s** | 529.9 | $MnO_2$ or other Mn oxide. Other metal oxide. | | 9.8 |
| | 530.5 | Metal oxides | 4.6 | |
| | 531.9 | R-$CO_3$, metal-OH, Si-O | 52.9 | 48.4 |
| **Mn2p3** | 641.7 | $MnO_2$, $Mn_2O_3$, or MnO(OH) | --- | 5.2 |

### 3.2. Effect of initial Mn concentration on long-term operation of a calcite contactor

Fig 3a shows the Mn concentrations measured in the effluents of the contactors fed with SFW containing 0.5 or 5 mg Mn $L^{-1}$ over 800 h of operation. For both tested conditions, the contactors were able to remove over 95% of dissolved Mn from the SFW, reaching effluent concentration below 45 μg Mn $L^{-1}$. This removal was achieved in the column fed with 0.5 mg Mn $L^{-1}$ from the beginning of the operation; nevertheless, the trend was different for the higher initial Mn concentration (i.e. 5.0 mg Mn $L^{-1}$): the stable condition was reached after 250 h of operation. Even

though Mn breakthrough was not observed in the effluent for any of the two columns after 800 h, hardness release declined after around 600 h of operation when the initial Mn concentration in the feed was 5.0 mg Mn $L^{-1}$ (Fig. 3b).

It is of interest to point out that no significant change of the color of the bed treating 0.5 mg Mn $L^{-1}$ was visually detectable. In contrast, the feed with 5 mg Mn $L^{-1}$ resulted in a significant change of the bed color (from milky white towards black-brownish) (Table 4). A possible explanation for the observed hardness decline is most likely the effect of MnOx present on the calcite surface, a statement supported by the EDX analysis. After long-term operation of the contactor, Mn accumulation at the calcite surface caused a deterioration of the calcite dissolution due to the coverage of the mass transfer boundary layer with Mn deposits, which impeded calcium diffusion from the calcite core through this newly formed layer. Consequently, after long-term operation calcite cannot be dissolved effectively and should be replaced by fresh media.

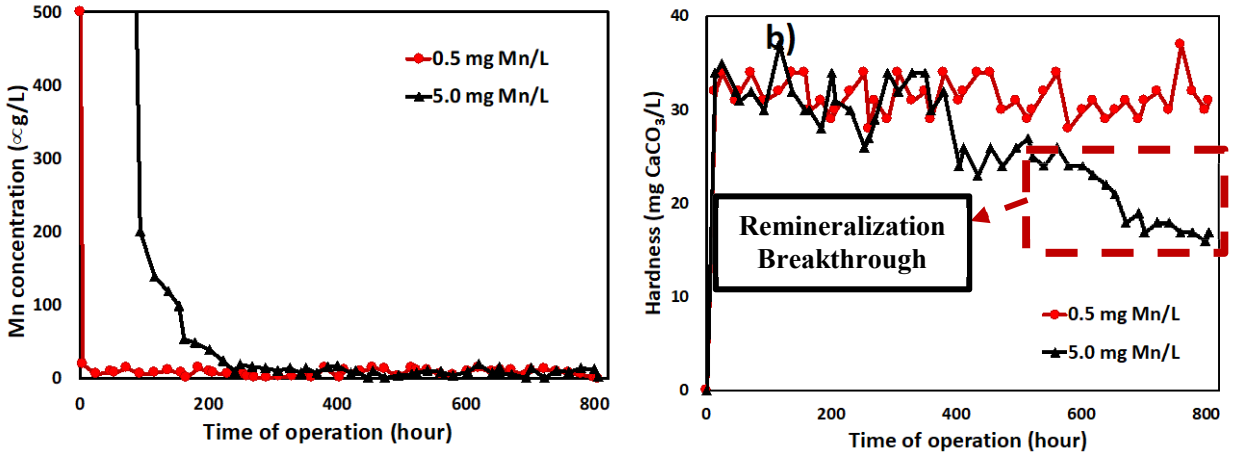


Figure 3: Concentrations of a) Mn and b) hardness measured over 800 h at the effluents (EBCT=10 min) of calcite contactors fed either with SFW containing 0.5 or 5 mg Mn $L^{-1}$

### 3.3. Effect of Mn solid-phase concentration on calcite dissolution

Fig. 4 illustrates the concentration of hardness released from the 5 columns which contained increasing Mn loadings (0 to 15 mg Mn $g^{-1}$ calcite). Indeed, in the case of fresh calcite (0 mg Mn

$g^{-1}$ calcite), the hardness release is higher than for the Mn loaded calcite (1-15 mg Mn $g^{-1}$ calcite). This phenomenon can be linked to the coating effect of Mn on the calcite surface which inhibited the dissolution of calcite. Thereby, it can be assumed that a Mn layer was formed in the solid-liquid interface where the dissolution reaction took place and, accordingly, deteriorated the calcite dissolution.

It should be pointed out that the highly loaded column was fed with Milli-Q water for 72 h (mini-column) or 800 h (column B) to investigate the Mn desorption rate and to determine the impact of the loaded media on the head loss, respectively. Results demonstrated no significant dissolution of Mn to the aqueous phase; the Mn deposit formed appeared to be very stable. Furthermore, no significant head loss was observed after the long-term operation of the Mn loaded column (i.e. 800 h).

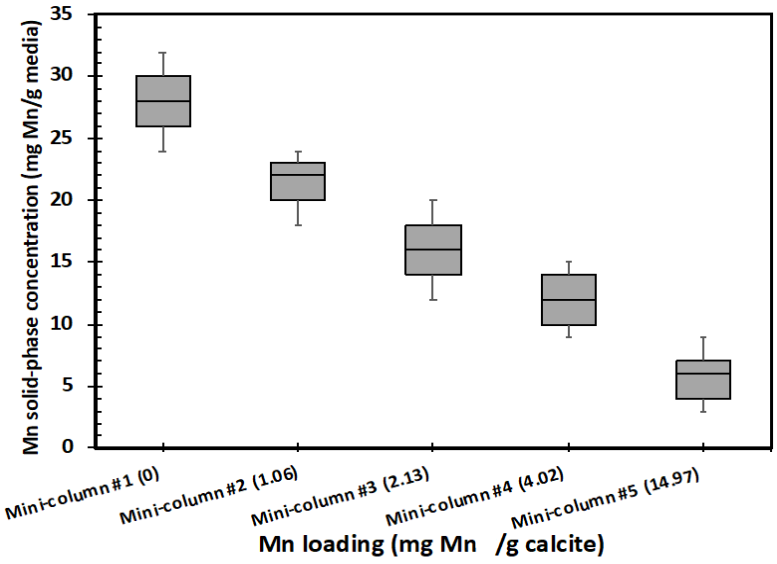


Figure 4: Hardness increase achieved by mini-columns containing increased Mn solid-phase concentrations on the calcite media (the numbers in parenthesis represent the Mn solid-phase concentration of the media (mg Mn $g^{-1}$ calcite). EBCT = 10 min and the feedwater had no hardness, pH = 6.0 and T = 23°C. Whisker-boxes provide averages, standard deviations and min/max values calculated over 72 h of operation.

### 3.4. Mn Sorption isotherm and kinetics

Fig. 5 presents Mn removal kinetics in a batch reactor containing 10 g $L^{-1}$ of a) fresh calcite and b) highly Mn loaded calcite (i.e. 15 mg Mn $g^{-1}$ calcite). As can be seen in Fig. 5a and 5b, for all the examined conditions, the required time to reach a stable Mn sorption regime on the calcite surface was approx. 24 h regardless of the Mn solid-phase concentration. However, when the Mn-loaded calcite was used, more efficient Mn uptake was observed compared to the fresh calcite. In the case of the fresh media, when the Mn concentration of the feed was increased from 100 to 10 000 µg Mn $L^{-1}$, Mn removal increased from 76% to 91%, respectively. One can note that the highest Mn removal (≥ 98%) was reached when the calcite was preloaded with 15 mg Mn $g^{-1}$ regardless of the initial Mn concentration. This observation confirms that the formed Mn layer favored the removal of the influent Mn concentration.

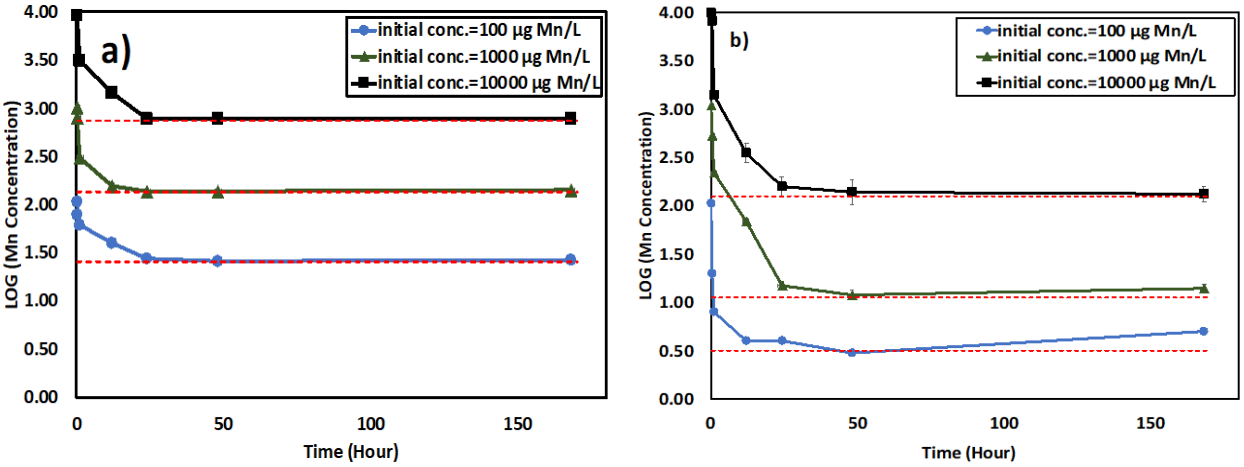


Figure 5: Impact of Mn solid-phase concentration on $Mn^{+2}$ removal by calcite in a mixed batch reactor for a) fresh calcite, b) Mn preloaded calcite (i.e.15 mg Mn $g^{-1}$ calcite)

### 3.5. Prediction of long-term operation of calcite contactor by simulations

The performance of the calibrated model is demonstrated in Figure 7 for the column fed with 5 mg Mn $L^{-1}$. Calibrated parameters were $k_{CAL} = 6 \times 10^{-6}\, M.s^{-1}$, $k_{MnCO3} = 10^{9.35X_{MnO2}-2.95}\, M.s^{-1}$, $k_{MnO2} = 5 \times 10^{-8}\, M.s^{-1}$ and $D_{barr} = 2 \times 10^{-11}\, m^2.s^{-1}$. The simulated Mn molar composition in

the $CaCO_3$ matrix near the outlet of the column was predicted to be 10% as $MnO_2$ and 90% as $MnCO_3$. The calibrated model resulted in good simulation of Mn experimental data. The model captured the hardness release decrease, though the simulated decrease slope was slightly smoother than the experimental one. The slight pH drop was captured as well; however, the simulated pH was higher than the experimental pH by 0.3 to 0.7 pH units. The pH discrepancy can be partly explained by the absence of atmospheric $CO_2$ input at the effluent in the model. The pH of the effluent samples might have been reduced by $CO_2$ input during processing, as they had a low buffer capacity.

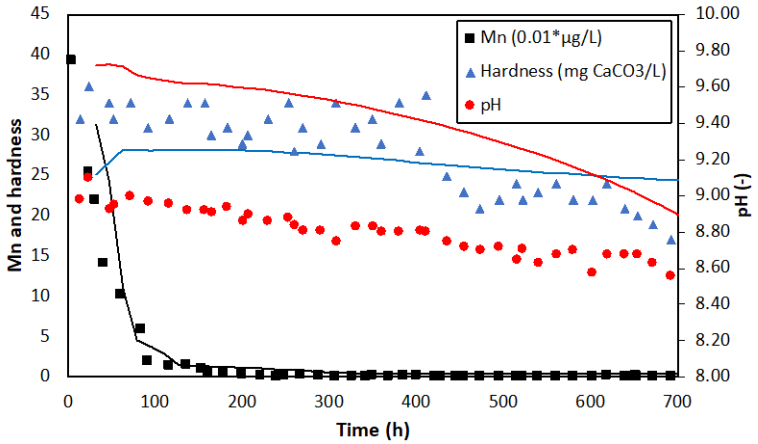


Figure 6: Calibrated model predictions for the hardness and manganese data for an EBCT=10 m of the calcite contactor over 700 h of operation. Feed = 5.0 mg Mn $L^{-1}$. The experimental data are shown by symbols while model predictions are provided as solid lines.

In order to assess the importance of recrystallization reactions in modelling Mn removal by calcite contactors, a sensitivity analysis was performed on the $MnO_2$ recrystallization rate using an influent with 5000 or 500 µg Mn $L^{-1}$ (Fig. 7). The recrystallization rate ranged from $5 \times 10^{-9}$ to $1 \times 10^{-6}$ $M.s^{-1}$, representing a very slow recrystallization kinetic (1% of Mn as $MnO_2$ on the media close to the outlet) or a very fast recrystallization kinetic (80% of Mn as $MnO_2$ on the media close to the outlet), respectively.

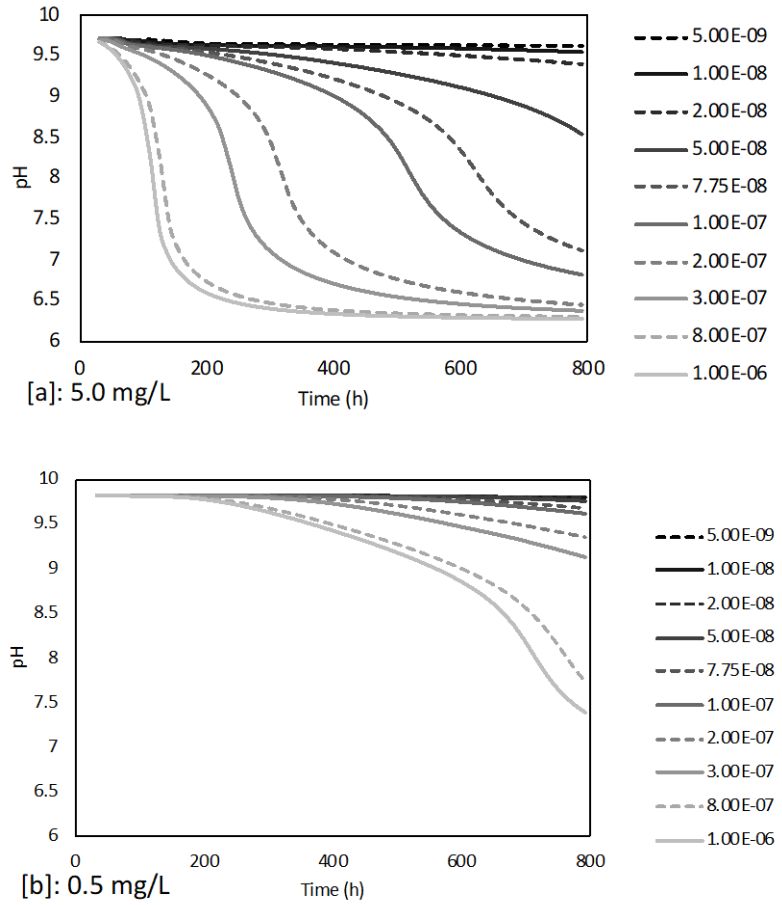


Figure 7: Effect of $MnO_2$ recrystallization rate (M/s, indicated in legend) on pH of the effluent, assuming an influent with a Mn concentration of (a) 5.0 mg Mn $L^{-1}$ or (b) 0.5 mg Mn $L^{-1}$.

The pH at the effluent of the calcite contactor was predicted to be highly influenced by the recrystallization rate for both of the initial Mn concentrations in the feed water (i.e. 500 and 5000 µg Mn $L^{-1}$). The fastest recrystallization rates simulated resulted in an unrealistically low pH (< 6.5 at 5000 µg Mn $L^{-1}$). This indicates that assuming the direct precipitation of $MnO_2$ or fast recrystallization into $MnO_2$ were not suitable hypotheses for modelling the calcite contactor. In the course of this study, the proposed modelling strategy consisted therefore of two main steps: (1) fast Mn removal by sorption and (2) the long-term behavior of the Mn solid phases in the contactor. As shown in Figure 6, this strategy employed with proper calibration led to realistic breakthrough

curves and $MnO_2$ content in the contactor. Indeed, the simulated $MnO_2$ proportion in Mn precipitate for the column fed with 5 mg Mn $L^{-1}$ was over 10%, which was sufficient to be detected by XPS analysis.

In order to apply the proposed model as a useful tool to design a calcite contactor and to predict its exhaustion further investigations are required in terms of calibration (using various initial Mn content in the feed water). In addition, performing additional mineralogical analyses at different points in the contactor and at different times of operation are recommended to substantiate the recrystallization hypothesis. Although the implementation of solely calcite media resulted in effective Mn removal, in the absence of $CO_2$ injection to the calcite column, the targeted hardness level (30 mg $CaCO^3$ $L^{-1}$) was not achieved when Mn content was very high in the feed. Thereby, in future work, the dissolution behavior of a blend of calcite/MgO will be studied by running a long-term calcite/MgO contactor.

## 4. Conclusion

This study set out to determine the adverse impact of the newly-formed manganese (Mn)-layer on calcite dissolution in a long-term operation of a calcite contactor. The main findings can be summarized as follow:

- The calcite contactor was able to remove ≥ 95% of dissolved Mn in a long-term operation (i.e. 800 h), regardless of the initial Mn concentration in the feed water.
- The targeted hardness level of the effluent stream (> 30 mg $CaCO_3$ $L^{-1}$) was reached when the Mn concentration of the feed was 0.5 mg $L^{-1}$. However, with 5 mg $L^{-1}$ of initial Mn content, a decrease in hardness release was reached after only 400 h of operation.

- Sorption experiments, XPS and EDX analyses showed that hardness decline was most likely due to the MnOx present on the calcite surface. This phenomenon was linked to the coating effect of Mn on the calcite surface which inhibited the dissolution of calcite. We suggested that an Mn layer was formed in the solid-liquid interface where the dissolution reaction took place and, accordingly, deteriorated the calcite dissolution.
- The implemented modelling strategy consisted of two steps: (i) fast Mn removal by sorption and (ii) slow crystallization of $MnCO_3$ as $MnO_2$. Including this last step was essential to properly model the observed pH behaviour of the effluent.

Clearly, further investigations will be needed to validate the recrystallization hypothesis via mineralogical analyses at different points in the contactor. In addition, an assessment of a long-term calcite/MgO contactor to achieve > 30 mg $CaCO_3$ $L^{-1}$ (when Mn content is very high in the feed water) is of interest. Work on those issues is ongoing and will be presented in future papers.

## Acknowledgements

This research was supported by the Canadian NSERC Discovery Grant Program (312139). The authors thank Mrs. M. Blais for the ICP-OES measurements carried out at the CREDEAU laboratories (a *Canadian Foundation for Innovation* funded infrastructure), Polytechnique Montreal, Canada.

# Appendix

## 1. Electron microscopy and elemental analysis

Scanning electron microscopy (SEM) images were taken at 250X magnification using a field emission gun electron microscope (model: JMS-7600 FEG-SEM, Jelo, USA). An energy dispersive spectrometer (model: Oxford X-Max silicon drift detector, Oxford Instrument, UK) was connected to the microscope to perform the elemental analysis of the surface of calcite media (EDX). The EDX analysis was carried out at the same magnification as the SEM analysis (250X), using a 15-kV accelerating voltage and a 20 mm working distance.

## 2. X-ray Photoelectron Spectrometry (XPS) analysis

X-ray Photoelectron Spectrometry (XPS) analysis was done on the surface of the fresh and Mn loaded calcite media. The experimental conditions of the XPS analysis are given in the following table.

| **Operational conditions** | **Data** |
|---|---|
| Apparatus | VG ESCALAB 3 MKII |
| Source | Al Kα |
| Power | 300 W (15 kV, 20 mA) |
| Pressure in analysis chamber | 3.0 x 10-9 Torr |
| Analysed surface | 2 mm x 3 mm |
| Electron takeoff angle | 0 degrees |
| Analysed depth | < 10 nm |
| Detection limit | ~ 0.1 % atomic |
| Survey scans energy: step size | 1.0 eV |
| Survey scans energy: pass energy | 100 eV |
| High resolution scans: energy step size | 0.05 eV |
| High resolution scans: pass energy | 20 eV |
| Background subtraction | Shirley method |
| Sensitivity factor table | Wagner |
| Charge correction with respect to C1s at | 285.0 eV |

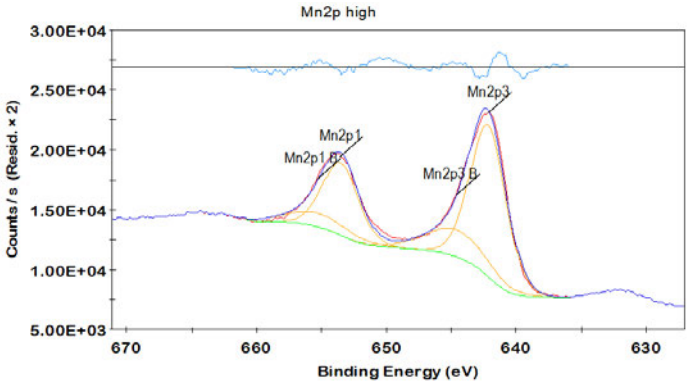


Figure: XPS analysis of the Mn loaded calcite media (15 mg/g) for the region of Mn oxides.

## References


AZIZ, H. A. & SMITH, P. G. 1992. The influence of pH and coarse media on manganese precipitation from water. *Water Research,* 26**,** 853-855.

AZIZ, H. A. & SMITH, P. G. 1996. Removal of manganese from water using crushed dolomite filtration technique. *Water Research,* 30**,** 489-492.

BAER, D. R., BLANCHARD, D. L., ENGELHARD, M. H. & ZACHARA, J. M. 1991. The interaction of water and Mn with surfaces of CaCO3: An XPS study. *Surface and Interface Analysis,* 17**,** 25-30.

BARBEAU, B., CARRIÈRE, A. & BOUCHARD, M. F. 2011. Spatial and temporal variations of manganese concentrations in drinking water. *Journal of Environmental Science and Health, Part A,* 46**,** 608-616.

BOUCHARD, M. F., SAUVÉ, S., BARBEAU, B., LEGRAND, M., BRODEUR, M.-È., BOUFFARD, T., LIMOGES, E., BELLINGER, D. C. & MERGLER, D. 2011. Intellectual impairment in school-age children exposed to manganese from drinking water. *Environmental health perspectives,* 119**,** 138.

CANADA, H. 2016. Manganese in drinking water. Federal-Provincial-Territorial Committee on Drinking Water. *In:* OTTAWA, O., CANADA (PP. 116) (ed.).

CARRIÈRE, A., BROUILLON, M., SAUVÉ, S., BOUCHARD, M. F. & BARBEAU, B. 2011. Performance of point-of-use devices to remove manganese from drinking water. *Journal of Environmental Science and Health, Part A,* 46**,** 601-607.

CHARLTON, S. R. & PARKHURST, D. L. 2011. Modules based on the geochemical model PHREEQC for use in scripting and programming languages. *Computers & Geosciences,* 37**,** 1653-1663.

CLAVEAU-MALLET, D., COURCELLES, B., PASQUIER, P. & COMEAU, Y. 2017. Numerical Simulations with the P-Hydroslag Model for Prediction of Phosphorus Removal by Steel Slag Filters. *Water Research,* 126**,** 421-432.

COMANS, R. N. J. & MIDDELBURG, J. J. 1987. Sorption of trace metals on calcite: Applicability of the surface precipitation model. *Geochimica et Cosmochimica Acta,* 51**,** 2587-2591.

DION, L.-A., SAINT-AMOUR, D., SAUVÉ, S., BARBEAU, B., MERGLER, D. & BOUCHARD, M. F. 2018. Changes in water manganese levels and longitudinal assessment of intellectual function in children exposed through drinking water. *NeuroToxicology,* 64**,** 118-125.

DOMENICO, P. A. & SCHWARTZ, F. W. 1998. *Physical and Chemical Hydrogeology,* New York, John Wiley & sons.

FARLEY, K. J., DZOMBAK, D. A. & MOREL, F. M. M. 1985. A surface precipitation model for the sorption of cations on metal oxides. *Journal of Colloid and Interface Science,* 106**,** 226-242.

FRANKLIN, M. L. & MORSE, J. W. 1983. The interaction of manganese(II) with the surface of calcite in dilute solutions and seawater. *Marine Chemistry,* 12**,** 241-254.

GAMBOU-BOSCA, A. & BÉLANGER, D. 2016. Electrochemical accessibility of porous submicron MnO2 spheres as active electrode materials for electrochemical capacitors. *Electrochimica Acta,* 201**,** 20-29.

GHANBARI, S. 2018. *Pilot study and modeling of remineralization of low-temperature desalinated water by calcite filtration.* M.Sc., Delft University of Technology, Delft.

HADDAD, M., OHKAME, T., BÉRUBÉ, P. R. & BARBEAU, B. 2018. Performance of thin-film composite hollow fiber nanofiltration for the removal of dissolved Mn, Fe and NOM from domestic groundwater supplies. *Water Research,* 145**,** 408-417.

KOTHARI, N. 1988. Groundwater, iron and manganese an unwelcome trio. *Water Engineering and Management; (USA)***,** Medium: X; Size: Pages: 25-26.

LETTERMAN, R. D., DRISCOLL, C. T., HADDAD, M. & HSU, H. A. 1987. Limestone bed contactors for control of corrosion at small water utilities. *Limestone bed contactors for control of corrosion at small water utilities.* US EPA. Water Engineering Research Laboratory.

MCBRIDE, M. B. 1979. Chemisorption and Precipitation of $Mn^{2+}$ at CaCO3 Surfaces1. *Soil Science Society of America Journal,* 43**,** 693-698.

PARKHURST, D. L. & APPELO, C. A. J. 1999. User's guide to PHREEQC (Version 2) - A computer program for speciation, batch-reaction, one-dimensional transport, and inverse geochemical calculations. *In:* SURVEY, U. S. G. (ed.). Denver.

PINGITORE, N. E., EASTMAN, M. P., SANDIDGE, M., ODEN, K. & FREIHA, B. 1988. The coprecipitation of manganese(II) with calcite: an experimental study. *Marine Chemistry,* 25**,** 107-120.

PLUMMER, L., PARKHURST, D. & WIGLEY, T. 1979. Critical review of the kinetics of calcite dissolution and precipitation. ACS Publications.

PLUMMER, L., WIGLEY, T. & PARKHURST, D. 1978. The kinetics of calcite dissolution in $CO_2$-water systems at 5 degrees to 60 degrees $^oC$ and 0.0 to 1.0 atm $CO_2$. *American journal of science,* 278**,** 179-216.

SHEMER, H., HASSON, D. & SEMIAT, R. 2013. Design Considerations of a Packed Calcite Bed for Hardening Desalinated Water. *Industrial & Engineering Chemistry Research,* 52**,** 10549-10553.

SILVA, A. M., CORDEIRO, F. C. M., CUNHA, E. C. & LEÃO, V. A. 2012a. Fixed-Bed and Stirred-Tank Studies of Manganese Sorption by Calcite Limestone. *Industrial & Engineering Chemistry Research,* 51**,** 12421-12429.

SILVA, A. M., CRUZ, F. L. S., LIMA, R. M. F., TEIXEIRA, M. C. & LEÃO, V. A. 2010. Manganese and limestone interactions during mine water treatment. *Journal of Hazardous Materials,* 181**,** 514-520.

SILVA, A. M., CUNHA, E. C., SILVA, F. D. R. & LEÃO, V. A. 2012b. Treatment of high-manganese mine water with limestone and sodium carbonate. *Journal of Cleaner Production,* 29-30**,** 11-19.

THORNTON, F. C. 1995. Manganese removal from water using limestone-filled tanks. *Ecological Engineering,* 4**,** 11-18.

TOBIASON, J. E., BAZILIO, A., GOODWILL, J., MAI, X. & NGUYEN, C. 2016. Manganese Removal from Drinking Water Sources. *Current Pollution Reports,* 2**,** 168-177.

VAN DER LAAN. H., V. O. J., VAN HOUWELINGEN. G., SOUSI. M., ZIJP. M., KOK. L., SCHOONDERWOERD. V. 2016. Search for the optimal remineralization technology. South Holland: Delft University of Technology.

WITHERS, A. 2005. Options for recarbonation, remineralisation and disinfection for desalination plants. *Desalination,* 179**,** 11-24.

YAMAUCHI, V., TANAKA, K., HATTORI, K., KONDO, M. & UKAWA, N. 1987. Remineralization of desalinated water by limestone dissolution filter. *Desalination,* 66**,** 365-383.

ZACHARA, J. M., COWAN, C. E. & RESCH, C. T. 1991. Sorption of divalent metals on calcite. *Geochimica et Cosmochimica Acta,* 55**,** 1549-1562.